Quasiparticle chirality in Epitaxial Graphene Probed at the Nanometer Scale

Ivan Brihuega, Pierre Mallet, Cristina Bena, Sangita Bose, Christian Michaelis, Lucia Vitali, François Varchon, Laurence Magaud, Klaus Kern, Jean-Yves Veuillen

Quasiparticle Chirality in Epitaxial Graphene Probed at the Nanometer Scale

I. Brihuega,[1] P. Mallet,[2,*] C. Bena,[3] S. Bose,[1] C. Michaelis,[1]
L. Vitali,[1] F. Varchon,[2] L. Magaud,[2] K. Kern,[1,4] and J. Y. Veuillen[2]

[1]*Max-Planck-Institut für Festkörperforschung, Heisenbergstrasse 1, D-70569 Stuttgart, Germany*
[2]*Institut Néel, CNRS-UJF, BP166, 38042 Grenoble, France*
[3]*Institut de Physique Théorique, CEA/Saclay, Orme des Merisiers, 91190 Gif-sur-Yvette, France*
[4]*Institut de Physique des Nanostructures, Ecole Polytechnique Fédérale de Lausanne, CH-1015 Lausanne, Switzerland*
(Dated: published on 14th November 2008 in Physical Review Letters 101, 206802 (2008)))

Graphene exhibits unconventional two-dimensional electronic properties resulting from the symmetry of its quasiparticles, which leads to the concepts of pseudospin and electronic chirality. Here we report that scanning tunneling microscopy can be used to probe these unique symmetry properties at the nanometer scale. They are reflected in the quantum interference pattern resulting from elastic scattering off impurities, and they can be directly read from its fast Fourier transform. Our data, complemented by theoretical calculations, demonstrate that the pseudospin and the electronic chirality in epitaxial graphene on SiC(0001) correspond to the ones predicted for ideal graphene.

PACS numbers: 73.20.-r, 68.37.Ef, 72.10.Fk

Graphene, one single layer of carbon atoms packed in a honeycomb structure, has two identical carbon atoms in each unit cell and thus two equivalent atom sublattices. This gives rise to an extra degree of freedom absent in conventional two-dimensional (2D) systems, and leads to exceptional electronic properties. The major consequence of the honeycomb structure is that the low energy quasiparticles of graphene are described by a Dirac-like Hamiltonian. The energy spectrum is thus linear, and consists of two Dirac cones centered at the opposite corners K and K' of the Brillouin zone. This is, however, insufficient to understand properly the specific electronic properties of graphene. Due to the presence of the two C atoms per unit cell, the quasiparticles have to be described by two-component wave functions, each component specifying the (complex) amplitude on each atomic sublattice. This results in an additional degree of freedom known as pseudospin. The projection of the pseudospin on the direction of the momentum defines the chirality of the quasiparticules; in graphene the direction of the quasiparticle pseudospin is parallel (positive chirality) or antiparallel (negative chirality) to their momentum [1, 2]. Within one single Dirac cone, electrons (or equivalently holes) of opposite direction have opposite pseudospin, but the same chirality. In graphene bilayer with Bernal stacking, chiral Dirac fermions are also found, but they are massive and their chirality differs from the one found in graphene monolayer [1, 2].

In order to fully exploit graphene in future electronic devices it is of primary importance to assess the chirality of the quasiparticles, since this feature is central to the transport properties. It is responsible for the new "chiral" quantum Hall effects (QHE) measured in exfoliated monolayer and bilayer graphene [3–5]. In epitaxial graphene multilayers on the SiC(000$\bar{1}$) face, Shubnikov-de-Haas oscillations and weak antilocalization effects consistent with the electronic chirality of "uncoupled" graphene layers [6, 7] have been reported, but surprisingly the QHE has not been yet observed [8]. Therefore, a direct measure of the electronic chirality in a single epitaxial graphene layer is essential. Here we show that the quasiparticles pseudospin - and the associated chirality - can be probed at the nanometer scale with a low temperature scanning tunneling microscope (STM). Our results on graphene monolayer on SiC(0001) are consistent with the electronic chirality of ideal graphene.

Epitaxial graphene was grown on a 6H-SiC(0001) substrate by thermal desorption of silicon at high temperatures, in ultra high vacuum (UHV) [9, 10]. Parameters were chosen to obtain a mixed surface with a similar coverage of monolayer and bilayer (with Bernal stacking) terraces, $\sim$ 50 nm wide. A carbon layer is present at the interface between graphene and the SiC. This layer is strongly bound to the substrate, and acts as a buffer layer with negligible interactions with the graphene layers [11]. Although not metallic, the carbon buffer layer has electronic states that give a significant contribution to the STM images [10, 12]. Our experiments were done using a home-made microscope operating at 4K in ultra-high vacuum. High bias STM images, as shown in Fig. 1(a), allow discriminating monolayer from bilayer graphene terraces due to the different interface states contribution [10].

Two groups have reported angle-resolved photoemission spectroscopy (ARPES) measurements on epitaxial graphene layers on SiC(0001). They demonstrate that the graphene layers are electron doped. The measured difference between the Fermi energy (E_F) and the Dirac energy (E_D) is $\sim$ 0.45 eV for a monolayer and $\sim$ 0.30 eV for a bilayer [13–15]. For graphene monolayer, a low energy linear dispersion has been found, a fingerprint of Dirac-like fermions [13, 14]. However, different results are obtained by the two groups concerning the crossing of the bands: An energy gap of 0.25 eV is found at the Dirac point by only one of the groups [14]. It has

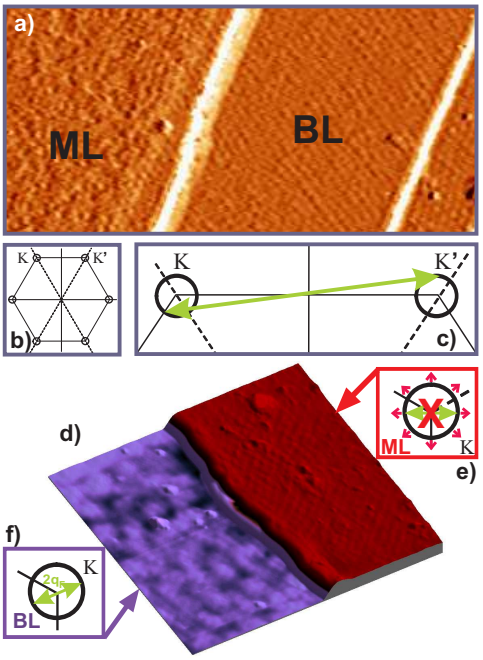

FIG. 1: (color online) (a) Constant current 90×43 nm^2 STM image of epitaxial graphene on SiC(0001), with two adjacent monolayer (ML) and bilayer (BL) graphene terraces. The spatial derivative of the image is shown, to enhance the corrugation due to the interface states which is higher on ML terraces [10]. Sample bias: +980 mV, tunneling current: 0.15 nA. (b) Schematic Fermi surface for electron-doped ML and BL graphene. (c) Illustration of an intervalley scattering process. (d) 3D rendered 50×50 nm^2 constant current image of two adjacent ML and BL terraces, taken at low sample bias (+ 1mV). A long wavelength scattering pattern is found on the BL terrace (left), and not on the ML terrace (right). Tunneling current: 0.2 nA. (e) Schematic of forbidden intravalley backscattering for ML graphene. Red arrows sketch the pseudospin direction. (f) Schematic of intravalley backscattering for BL graphene.

been proposed by the authors that the gap arises from a substrate-induced breaking of the sublattice symmetry of graphene. ARPES, also shows that the Fermi surfaces (FSs) of monolayer and bilayer graphene on SiC(0001) are essentially identical [15, 16].They consist of two tiny circular pockets, of radius q_F, surrounding the K and K' points [Fig. 1(b), six pockets are sketched to account for the symmetry of the Brillouin zone].

At low sample bias (a few mVs), the STM probes essentially the electronic states of the FS, and a constant current image reflects a map of the surface local density of states (LDOS) at E_F [17]. In a 2D system such as graphene, low bias images probe the quantum interferences (QIs) arising from elastic scattering of surface quasiparticles at static defects [18]. Such QIs are related to the Friedel oscillations in 2D metals. In a simple picture, any impurity scattering between two states $\overrightarrow{k}$ and $\overrightarrow{k}'$ of the FS should give rise to LDOS spatial modulations with wavevector $\overrightarrow{k}' - \overrightarrow{k}$, with a scattering probability depending on the topology of the FS. For a circular FS of radius k_F, scattering between states $\overrightarrow{k}_F$ and states $-\overrightarrow{k}_F$ (termed backscattering in the following) are the most efficient processes due to enhanced phase space, resulting in LDOS modulations with wavector $2k_F$ [18, 19].

For the FS sketched in Fig. 1(b), and depending on the impurity potentials present in the system, we may expect elastic electron scattering processes between the two non-equivalent Dirac cones at K and K' (i.e. intervalley scattering) as depicted in Fig. 1(c), together with elastic scattering processes between states located on the same Dirac cone (i.e. intravalley scattering). Figure 1(d) is a constant current STM image taken at +2mV that includes two adjacent graphene monolayer and bilayer terraces. A striking difference is measured in the LDOS patterns between the left and right terraces. A clear long-range modulation, of wavelength 5.2±0.3 nm, is found on the graphene bilayer terrace. This modulation has already been reported by Rutter et al. [12], and is attributed to quantum interferences of wave vector $2q_F$ due to intravalley backscattering between states $\overrightarrow{q}_F$ and states $-\overrightarrow{q}_F$ within one single pocket [Fig. 1(f)]. Surprisingly, we do not find such LDOS modulation on the monolayer, which is puzzling if we keep in mind that the two systems have almost the same FS.

The lack of LDOS modulation of wave vector $2q_F$ for the monolayer implies that QIs associated with intravalley backscattering are virtually absent. It has been reported that wave function symmetries may lead to selection rules that can prevent QIs, for instance in systems with strong spin-orbit coupling where the electronic spin governs the elastic scattering processes [20, 21]. In the present case, the absence of QIs in graphene monolayer is associated to the pseudospin instead of real spin. Intuitively, this is because the pseudospin of the backscattered wave is opposite to that of the incident wave, so that their overlap should be zero [see Fig. 1(e)]. For a scattering potential with range larger than the C-C distance (which leads to scattering without pseudospin-flip), it has been shown that intravalley backscattering processes and the associated QIs are strictly forbidden in monolayer graphene [22, 23]. On the contrary, the electronic chirality does not prevent intravalley backscattering in bilayer graphene [Fig. 1(f)] [24].

For both monolayer and bilayer epitaxial graphene on SiC(0001), previous STM experiments have reported that atomic-size impurities give rise to short-wavelength modulations of the LDOS, associated with intervalley scattering [10, 12]. According to Ando et al. [22], such impurities, acting as short-range potentials, should also allow intravalley backscattering, which raises the question of possible QIs of wave vector $2q_F$. Recent theoretical studies show that for a general impurity potential, LDOS modulations with wave vector $2q_F$ should exist for

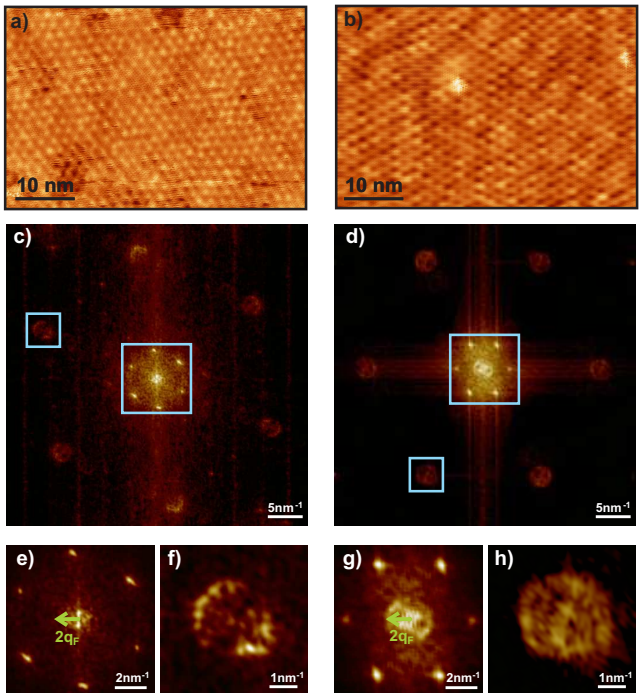

FIG. 2: (color online) (a),(b) Low-bias STM images of 50 nm wide monolayer (a) and bilayer (b) terraces. Sample bias and tunneling current are respectively +2 mV and 0.4 nA for (a), +4 mV and 0.13 nA for (b). (c),(d) Two-dimensional fast Fourier transform (FFT) maps of the STM images (a) and (b). (e) Central region of (c), showing no intravalley-backscattering related ring (the green arrow points out the position where such a ring should appear). (f) One of the outer pockets of (c). (g) Central region of (d), showing a clear ring-like feature of radius $2q_F$ related to intravalley-backscattering. (h) One of the outer pockets of (d). Outer pockets shown in (f) and (h) are centered at the K (or K') point and result from intervalley scattering.

graphene monolayer, but they should be strongly attenuated [25–27], with a $1/r^2$ decay law instead of the $1/r$ law found in conventional 2D systems. On the other hand, a $1/r$ decay law is obtained for the QIs due to intravalley backscattering in a graphene bilayer, and also for the QIs due to intervalley scattering for both monolayer and bilayer graphene. In reference [25] one of us showed that the $1/r^2$ decay law should have a clear impact on the 2D Fourier transform (FT) of the LDOS modulations: while on bilayer graphene the efficiency of intravalley backscattering should give rise to a central ring of radius $2q_F$ in the FT map similar to the one observed for conventional 2D systems, the strong attenuation of intravalley backscattering on monolayer graphene should generate a FT image with no central ring [25].

In the following, we present high resolution fast Fourier transform (FFT) of STM images recorded at low sample bias on 50 nm wide graphene terraces. We first show the real-space images, for graphene monolayer [Fig. 2(a)] and graphene bilayer [Fig. 2(b)]. Note that both images exhibit a triangular pattern of periodicity ~ 1.9 nm which is related to the interface reconstruction [10, 12], and which appears as a sextuplet of bright spots in the corresponding FFT images [Figs. 2(c) and 2(d)].

The central region of the FFT in Figs. 2(c) and 2(d) is related to intravalley scattering: a clear ring-like feature of average radius 1.2 nm^{-1} is found for the bilayer [Figs. 2(d) and 2(g)]. This radius value is in agreement with the value given in ref. [12], and with the $2q_F$ value derived from ARPES [13, 14]. On the monolayer terrace, no central ring is found [Figs. 2(c) and 2(e)], despite the unprecedented momentum resolution obtained here. This has been checked on many different monolayer terraces (see also the EPAPS document [28]), and we conclude that the result is robust and systematic. As discussed above, pseudospin and electronic chirality are the key parameters for the absence (presence) of the central ring in the FFT image of monolayer (bilayer) graphene.

In the high frequency regions of the FFTs of Figs. 2(c) and 2(d), we find six outer pockets with ring-like shapes centered at $K(K')$ points. They result from intervalley scattering, associated to real space LDOS modulations with a $(\sqrt{3}\times\sqrt{3})R30°$ periodicity with respect to graphene [10, 12]. As shown in Figs. 2(f) and 2(h), the intensity of the high frequency rings in the FFT is not isotropic. The anisotropy is much more pronounced for graphene monolayer, for which a splitting of each ring into two arcs is found [Fig. 2(f))]. This splitting is discussed in more detail in the EPAPS document [28].

The experimental results are compared with T-matrix calculation made along the lines of Ref. [25] (see also the EPAPS document [28]). Figure 3(a) is the FT of a calculated LDOS map at E_F for monolayer graphene with $E_D = E_F$-0.45 eV, in the presence of a single localized impurity. It is clear that no central $2q_F$ ring is generated in this case. This is the signature of LDOS modulations resulting from inefficient intravalley backscattering, and it is the most direct fingerprint of graphene's pseudospin and chirality [25]. This is in very good agreement with the experimental absence of the central ring [Fig. 2(e)]. Also, the high frequency split rings, resulting from intervalley scattering, are nicely reproduced by the theoretical calculation. The splitting of the rings is another consequence of the quasiparticle chirality [28].

Figure 3(b) is an equivalent map as Fig. 3(a) but for a graphene bilayer, with $E_D = E_F$-0.3 eV. From ARPES it is known that the two layers have a different electron density, giving rise to a gap at E_D of about 0.1 eV [15]. The asymmetry between the two layers has been included in the present calculation. Note the appearance of the inner ring of radius $2q_F$, as well as the presence of the outer rings which have not obvious splitting (a faint intensity remains perpendicularly to the ΓK and $\Gamma K'$ directions). The agreement with the experimental FFT is excellent.

Finally, we propose the use of STM to check any possible breaking of graphene's sublattice symmetry. To this

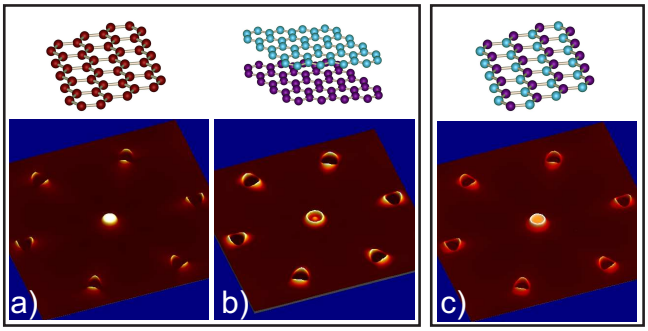

FIG. 3: (color online) (a-c) Theoretical calculation of the Fourier Transform (FT) of the LDOS at E_F for different graphene layers with a single delta-function impurity. (a) 3D rendered FT map for graphene monolayer with a Dirac energy $E_D = E_F - 0.45$ eV. The calculation predicts no central ring of radius $2q_F$, showing the unefficiency of intravalley backscattering. (b) Same representation as (a) for a bilayer, showing a clear central $2q_F$ ring. $E_D = E_F - 0.3$ eV. An asymmetry of ~ 0.1eV between the two layers has been included, to account for the different electron density reported by ARPES (12,13). (c) Same representation as (a) for an asymmetric monolayer, with $E_D = E_F - 0.45$eV. A site energy difference of 0.25 eV is introduced between the carbon atoms of each unit cell, and the impurity is placed on a carbon atom with high site energy. The symmetry breaking between the two carbon sublattices restores the efficiency of intravalley backscattering as shown by the reappearance of a central ring in the FT map.

end, we have calculated the FT of the LDOS map for a monolayer with the same parameters as in Fig. 3(a), but including an arbitrary sublattice asymmetry of 0.25 eV, which is the gap value measured by Zhou et al. [14]. The calculation shows a clear inner ring in the FT, corresponding to efficient QIs due to intravalley backscattering [28]. This dramatically illustrates the effect of the asymmetry on the FT STM data since this ring is absent in the symmetrical case [Fig. 3(a)]. The data of Fig. 3(c) are for a defect on one sublattice, but we found that the shape of the ring depends on the location of the scattering potential [28]. Due to the large size of the images it is likely that a distribution of defects is present in the experimental data. Calculations indicate that a large sublattice asymmetry (leading to a gap of 0.6 eV) should be readily detected in FT-STM images, but that for a moderate asymmetry (as for Fig. 3(c)) the intensity of the ring could depend on the defect configuration. Since we have taken images in many different surface areas without detecting any ring, we believe that our data are rather consistent with a symmetrical monolayer, although a small asymmetry can not be totally ruled out.

In summary, by analyzing the Fourier transform of low bias STM images, we have demonstrated that the pseudospin and the chirality of epitaxial graphene quasiparticles can be probed directly at the nanometer scale. We show that graphene monolayer on SiC(0001) exhibits the chirality of an ideal graphene sheet. Together with the previous evidence by ARPES of the low energy linear spectrum, a complete assessment of the Dirac nature of the quasiparticles in this system is obtained.

We thank D. Mayou for helpful discussions, F. Hiebel for participating to sample preparation, R. Cox for careful reading of the manuscript and the French ANR (programme Blanc) for partial financial support of this work. C. B. and I. B. were supported by a Marie Curie action under the Sixth Framework Programme.

* electronic address: pierre.mallet@grenoble.cnrs.fr

[1] A. K. Geim and K. S. Novoselov, Nature. Mater. **6**, 183 (2007)
[2] M. I. Katsnelson, K. S. Novoselov and A. K. Geim, Nature Phys. **2**, 620 (2006)
[3] K. S. Novoselov et al., Nature **438**, 197 (2005)
[4] Y. B Zhang, Y.-W. Tan, H. L. Stormer and P. Kim, Nature **438**, 201 (2005)
[5] K. S. Novoselov et al., Nature Phys. **2**, 177 (2006)
[6] C. Berger et al., Science **312**, 1191 (2006)
[7] X. Wu, X. Li, Z. Song, C. Berger and W.A. de Heer, Phys. Rev. Lett. **98**, 136801 (2007)
[8] W.A. de Heer et al., Solid State Comm. **143**, 92 (2007)
[9] I. Forbeaux, J.-M. Themlin and J.-M. Debever, Phys. Rev. B **58**, 16396 (1998)
[10] P. Mallet et al, Phys. Rev. B **76**, 041403(R) (2007)
[11] F. Varchon et al., Phys. Rev. Lett. **99**, 126805 (2007)
[12] G. M. Rutter, J. N. Crain, N. P. Guisinger, T. Li, P. N. First and J. A. Stroscio, Science **317**, 219 (2007)
[13] A. Bostwick, T. Ohta, T. Seyller, K. Horn and E. Rotenberg, Nature Phys. **3**, 36 (2007)
[14] S.Y. Zhou et al, , Nature Mater. **6**, 770 (2007)
[15] T. Ohta, A. Bostwick, T. Seyller, K. Horn and E. Rotenberg, Science **313**, 951 (2006)
[16] A. Bostwick et al., New Journ. of Phys. **9**, 385 (2007)
[17] J. Tersoff and D. R. Hamann, Phys. Rev. Lett. **50**, 1998 (1983)
[18] M. F. Crommie, C. P. Lutz and D. M. Eigler, Nature **363**, 524 (1993); Y. Hasegawa and Ph. Avouris, Phys. Rev. Lett. **71**, 1071 (1993)
[19] P. T. Sprunger, L. Petersen, E. W. Plummer, E. Laegsgaard and F. Besenbacher, Science **275**, 1764 (1997)
[20] L. Petersen, L. Bürgi, H. Brune, F. Besenbacher and K. Kern, Surf. Sci. **443**, 154 (1999); L. Petersen and P. Hedegård, Surf. Sci. **459**, 49 (2000)
[21] J. I. Pascual et al., Phys. Rev. Lett. **93**, 196802 (2004)
[22] T. Ando, T. Nakanishi and R. Saito, J. Phys. Soc. Jpn. **67**, 2857 (1998)
[23] M. I. Katsnelson and K. S. Novoselov, Solid State Comm. **143**, 3 (2007)
[24] M. I. Katsnelson, Phys. Rev. B **76**, 073411 (2007)
[25] C. Bena, Phys. Rev. Lett. **100**, 076601 (2008)
[26] E. Mariani, L. I. Glazman, A. Kamenev and F. von Oppen, Phys. Rev. B **76**, 165402 (2007)
[27] V. V. Cheianov and V. I. Fal'ko, Phys. Rev. Lett. **97**, 226801 (2006)
[28] See EPAPS Document No. —— for more details. For more information on EPAPS, see http://www.aip.org/pubservs/epaps.html.

Supporting Material of

"Quasiparticle Chirality in Epitaxial Graphene Probed at the Nanometer Scale",

I. Brihuega et al.

Experimental method

Synthesis of epitaxial graphene has been performed at Institut Néel, Grenoble, France. The details of the growth process and characterization of our atomically thin graphene samples have been discussed elsewhere [1]. Low temperature STM measurements have been done at Max Planck Institute, Stuttgart, Germany. After air exposure during the travelling time, the clean surface has been recovered in the UHV-STM chamber using a smooth annealing at 300-400°C. LDOS maps at the Fermi energy were obtained at 4 K (with a base pressure lower than 5.0×10^{-11} mbar), by recording standard constant current images at low sample bias (in the mV range) [2]. All measurements were performed in the tunnelling regime (i.e. under tunnelling conditions for which an exponential dependence of the tunnelling current with distance and reasonable work function values -between 3.5 and 5 eV- are obtained) at low enough currents (<1nA). Under these tunnelling conditions our results were completely independent of the tunnelling current used.

As indicated in the main text, a convenient way to differentiate monolayer areas from bilayer areas in large scale images is to take advantage of the larger interface contribution at high sample bias. We have cross-checked these observations by investigating the atomic contrast in the STM images [1, 3-5]. As shown on Fig. S1, high resolution images taken at atomic scale show the graphene lattice periodicity of 2.45 Å for monolayer and bilayer terraces. However, the contrast is markedly different, with a triangular pattern on graphene Bernal-stacked bilayer (upper-right image), and with a perfect honeycomb-like pattern on graphene monolayer (lower-

right image). This allows us to unambiguously discriminate monolayer terraces from bilayer terraces.

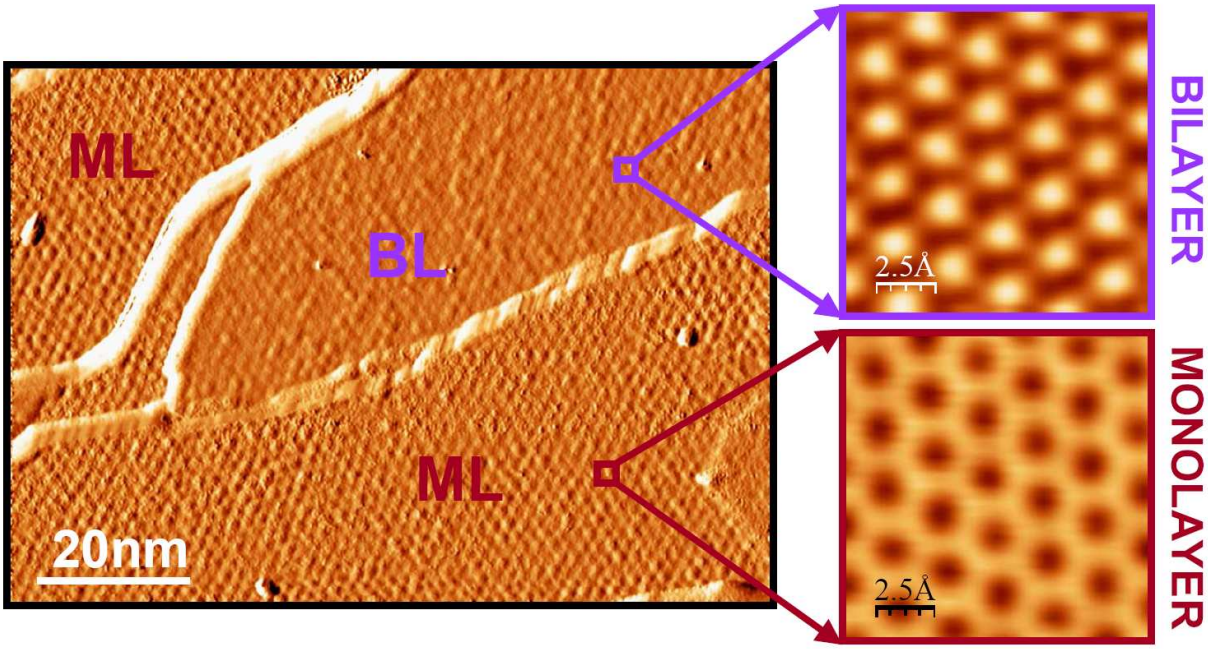

Fig. S1. A large scale constant-current STM image of our graphitized SiC(0001) sample, exhibiting monolayer (ML) and bilayer (BL) graphene terraces. Image size: 100 x 70 nm^2, sample bias +100mV, tunneling current 0.1 nA. The two images with atomic resolution sketched on the right correspond to images of the boxed areas on the left image. Sample bias and tunnelling current are respectively -50 mV and + 1.0 nA for the upper-right image, and -125 mV and + 0.1 nA for the lower-right image.

Large images (typically 50 nm wide) with a large number of points (up to 2048 points per line) were acquired to get sufficient resolution - and range - in the fast Fourier transform (FFT) images [6]. It takes only a few minutes (typically 20 minutes) to get such an image. This relatively short acquisition time allows for the investigation of many different spots on the

sample in order to verify that the FFT results were not dependent on a specific (local) form of disorder. The data were processed using the WsXM software [7].

Intervalley scattering in the monolayer

Figure S2(a) shows a 30x50 nm² image of a monolayer area taken at low bias. Figure S2(c) is a zoom-in on an area of size 6.3 x 6.3 nm². The honeycomb contrast (where all C atoms of the graphene layer are visible), which is typical for a graphene monolayer, is clearly seen at this scale. Also visible in the lower part of Fig. S2(b) is the $\sqrt{3}x\sqrt{3}R(30°)$ superstructure commonly found around point defects in monolayer and bilayer graphene [1,3]. It results from elastic electron scattering between the non equivalent K and K' valleys of the band structure of graphene (also called intervalley scattering). The Fermi contours at K and K' points are to first approximation circles with radius q_F (see Fig. 1). In a simple picture, the intervalley scattering events should therefore give rise to circles with radius $2q_F$ centered at the K and K' points of the surface Brillouin zone (SBZ) in the FFT of low-bias STM images [1, 3]. Indeed, structures that appear to be circular (indicated by arrows) are detected close to the K (K') points of the SBZ in the FFT of the STM image shown in Fig. S2(c). One notices however that these circles are not complete (see an expanded view in figure S2(d)): for any circle around K (K'), there is a line with minimum intensity, perpendicular to the ΓK (or ΓK') direction and going through the K (K') point, which divides the circle into an inner and an outer part. The same feature is observed in Fig. 2(f), and it is characteristic of the monolayer (it is not found for the bilayer, see Fig. 2(h)).

This peculiar split structure is also obtained in the computed FT-STM image of the monolayer shown in Fig. S2(d). It is again a consequence of the particular quasiparticle chirality in single-layer graphene. This conclusion stems from the fact that the split structure is absent in FT-STM images of bilayer graphene, either in the measurements (Fig. 2(h)) or in the calculations

([8] and Fig. 3(b)), despite the similarity between the Fermi surface of the two phases. In the calculated FT image of monolayer graphene, the signal intensity of the outer pockets in the direction perpendicular to ΓK is lower than 4% of the value along the ΓK direction. For bilayer graphene, a 40% intensity ratio between directions perpendicular and parallel to ΓK is still observed. Hence the chirality of the single layer graphene is reflected in various features of the FT-STM images: the absence of a circle around the Γ point and the split structures close to the K (K') points.

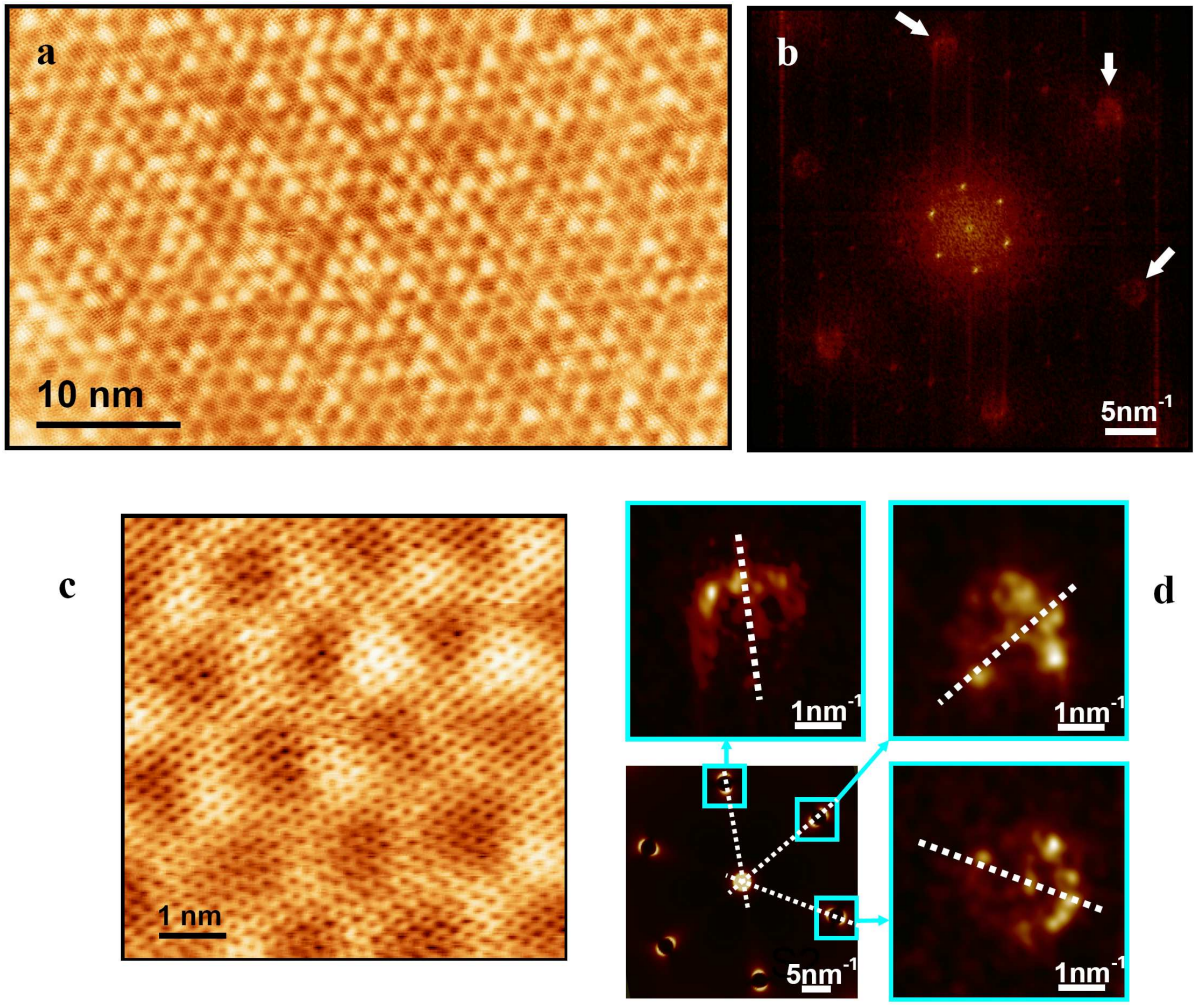

Fig. S2. STM analysis of the quantum interferences related to intervalley scattering in graphene monolayer**.** (**a**) 30 × 50 nm² image of a monolayer terrace at 4.5 K, sample bias: -2 mV, tunnelling current: 0.4 nA. (**b**) Fast

Fourier transform of the image shown in (a). Note again the absence of a ring at the centre. The arrows point to pockets related to intervalley scattering, that surround the K (K') points of the surface Brillouin zone. (**c)** 6.3 x 6.3 nm² numerical zoom-in of (a), exhibiting the honeycomb atomic contrast and the intervalley scattering-related $\sqrt{3}\times\sqrt{3}R(30°)$ real-space superstructure. (**d**) Zoom-in on the pockets marked by arrows in (b), together with a two-dimensional view of the computations of the Fourier transform STM image for a monolayer (same data as Fig. 4(a)). The dashed lines mark the different ΓK (or ΓK') directions of the surface Brillouin zone. Note that the pockets present a vanishing intensity in the directions perpendicular to the ΓK (ΓK') directions.

T-matrix calculations of the FT-STM images

We compare our experimental results to theoretical calculations performed using a T-matrix approximation. For the details of the procedure see references [8-10]. It is sufficient to note here that the FT-STM images are obtained by computing the trace of a convolution of two free Green's functions of graphene and the T-matrix, which incorporates the effect of the scattering potential. In general we focus on a delta-function impurity potential situated on one atom, which makes the T-matrix diagonal in the sublattice basis, and independent of momentum. The parameters we use in our evaluations of the LDOS for monolayer (ML) graphene correspond to a Dirac point at -0.45eV below the Fermi surface [11], with the FT-STM images evaluated at the Fermi surface. A quasiparticle inverse lifetime of 30meV is introduced to avoid divergences in the calculation; this translates into 30meV broadening of the peaks observed in the FT-STM images of Fig. 3.

For the graphene monolayer with an asymmetry between the two carbon sublattices, the computed FT-STM images actually depend on the site where the impurity resides. The FT-STM image depicted in figure 3(c) corresponds to a defect on the sublattice with the highest on-site energy (sublattice A), and in this case the asymmetry gives rise to a positive ring-like contribution at $2q_F$, superimposed over the central disk associated to the attenuated Friedel

oscillations. This is the configuration we have chosen to present in the main text because it illustrates most clearly the effect of the symmetry breaking. It turns out however that for a defect on a site of the other sublattice (sublattice B), the asymmetry results in a negative ring-like contribution to the FT-STM signal, superimposed over the central disk. Nevertheless, the non-equivalency between the two sublattices leads in both cases to standing wave patterns around the defect that will be decaying as 1/r. This is at variance with the case of a symmetrical monolayer where long wavelength LDOS oscillations decaying as1/r are absent due to a cancelation of the two sublattices contributions [8, 12, 13].

To model the situation in real samples, we have considered that: (i) Atomic resolution images show a honeycomb contrast, which indicates that the LDOS's on A and B sublattices are similar close to the Fermi level. Adsorption of impurities should thus occur equally on both sublattices. (ii) Images of ML samples of different origins [1, 5] suggest that there are different kinds of (native) localized defects (of unknown structure). Therefore, the conclusions stated in the main text derive from numerical simulations of the central spot of the FT-STM images for different structures of point defects where a given localized potential is placed on a: A site, on a B site or on two closely spaced A and B sites.

For bilayer graphene we consider that, in agreement with ARPES experiments [14], the lower layer (upper layer) has a chemical potential of -350 meV (-240 meV), with the Dirac point at -295meV and a gap of 110 meV. The impurity is chosen to lay on a site in the upper layer which is not coupled with a site in the bottom layer. The FT-STM images are again evaluated at the Fermi level in the top layer. The interlayer coupling is taken to be 600meV, while the intralayer hopping parameter is taken to be 3eV for both monolayer and bilayer graphene.

References:

[1] P. Mallet et al., Phys. Rev. **B76**, 041413(R) (2007)

[2] J. Tersoff and D.R. Hamann, Phys. Rev. Lett. **50**, 1998 (1983).

[3] G.M. Rutter, J.N. Crain, N.P. Guisinger, T. Li, P.N. First and J.A. Stroscio, Science **317**, 219 (2007)

[4] V.W. Brar et al., Appl. Phys. Lett. **91**, 122102 (2007)

[5] P. Lauffer et al., Phys. Rev. B **77**, 155426 (2008)

[6] L. Petersen et al., Phys. Rev. **B57**, R5868 (1998).

[7] I. Horcas et al., Rev. Sci. Instrum. **78**, 013705 (2007)

[8] C. Bena, Phys. Rev. Lett. **100**, 076601 (2008)

[9] C. Bena and S. Kivelson, Phys. Rev. B **72**, 125432 (2005).

[10] W. Ziegler et. al., Phys. Rev. B. **53**, 8704 (1996).

[11] A. Bostwick et al, New Journal of Physics **9**, 385 (2007).,

[12] T. Pereg-Barnea and A. H. MacDonald, Phys. Rev. B **78**, 014201 (2008)

[13] C. Bena, arXiv:0807.1981.

[14] T. Ohta et al., Science **313**, 951 (2006)